Irradiated Mammary Spheroids Elucidate Mechanisms of Macrophage-Mediated Breast Cancer Recurrence

Benjamin C. Hacker[1], Dana C. Herman[2], Erica J. Lin[3], Alyssa M. Questell[4], Rebecca J. Hedges[1], Marjan Rafat[1,4,5,*]

[1]Department of Chemical and Biomolecular Engineering, Vanderbilt University, Nashville, TN, USA

[2]Department of Biochemistry, Vanderbilt University, Nashville, TN, USA

[3]Department of Biological Sciences, Vanderbilt University, Nashville, TN, USA

[4]Department of Biomedical Engineering, Vanderbilt University, Nashville, TN, USA

[5]Department of Radiation Oncology, Vanderbilt University Medical Center, Nashville, TN, USA

*Author for correspondence: Marjan Rafat, PhD, Engineering and Science Building, Rm. 426, Vanderbilt University, Nashville, TN 37212. Phone: (615) 343-3389, Fax: (615) 343-7951, E-mail: marjan.rafat@vanderbilt.edu

Abstract

While most patients with triple negative breast cancer receive radiotherapy to improve outcomes, a significant subset of patients continue to experience recurrence. Macrophage infiltration into radiation-damaged sites has been shown to promote breast cancer recurrence in pre-clinical models. However, the mechanisms that drive recurrence are unknown. Here, we developed a novel spheroid model to evaluate macrophage-mediated tumor cell recruitment. We first characterized infiltrating macrophage phenotypes into irradiated mammary tissue to inform our model. We then established spheroids consisting of fibroblasts isolated from mouse mammary glands. We observed that tumor cell motility toward irradiated spheroids was enhanced in the presence of a 2:1 ratio of pro-healing:pro-inflammatory macrophages. We also measured a significant increase in interleukin 6 (IL-6) secretion after irradiation both *in vivo* and in our model. This secretion increased tumor cell invasiveness, and invasion was mitigated by neutralizing IL-6. Taken together, our work suggests that interactions between infiltrating macrophages and damaged stromal cells facilitates breast cancer recurrence through IL-6 signaling.

Key words

Macrophages, interleukin 6, triple negative breast cancer, irradiation, myeloid-stromal interactions, tumor cell recruitment, spheroid

Introduction

Breast cancer is the most diagnosed form of cancer—it is estimated that almost 300,000 American women will be diagnosed with the disease in 2022[1]. Approximately 15% of breast cancer patients are diagnosed with triple negative breast cancer (TNBC), a particularly aggressive subtype. To treat this disease, patients elect to undergo chemotherapy, surgery, and radiation therapy (RT)[2]. RT typically produces positive outcomes for a majority of patients[3,4]. However, an emerging body of literature implicates RT in contributing to cancer recurrence. Up to 20% of patients will experience locoregional recurrence after RT, and this may be correlated to patient immune status[2,5–7].

The impact of normal tissue radiation damage on cancer recurrence is currently understudied. Previous pre-clinical studies have linked radiation to tumor spread. For example, irradiation of mammary stroma induced breast cancer in injected epithelial cells[8]. However, radiation damage alone does not dictate recurrence. Radiation-induced metastasis of TNBC cells to the lung was shown to be facilitated by macrophages[9]. Pre-irradiation of tumor beds led to myeloid cell infiltration and then tumor cell growth due to matrix degradation[10]. More recently, macrophages were shown to promote tumor cell recurrence following normal tissue radiation damage[5]. However, the contribution of stromal-macrophage interactions to breast cancer recurrence following normal tissue radiation remain unknown.

Spheroid models provide an avenue to determine mechanisms of recurrence,[11] and their increased biological relevance compared to monolayer studies allows for insights into cell movement, direct cell-cell interactions, and cell-extracellular matrix (ECM) interactions[12–14]. Spheroid models complement *in vivo* models, and they serve as a crucial tool to design well-controlled and robust studies. In this study, we developed a novel primary fibroblast spheroid model to evaluate the effect of radiation damage on stromal-macrophage interactions that drive recurrence. We first characterized *in vivo* macrophage infiltration to inform our model parameters.

We then used our spheroid model to determine the contributions of irradiated normal tissue and macrophage infiltration to TNBC recurrence.

Results and Discussion

In vivo characterization of infiltrating macrophages and cytokine secretion resulting from radiation damage

We characterized the phenotypes of macrophages that infiltrated mouse mammary fat pads (MFPs) in a model of radiation-induced recurrence (**Figure 1A**)[5]. We defined pro-inflammatory M1 macrophages as $CD45^+CD11b^+F4/80^+$ cells expressing high levels of iNOS, CD86, CD64, or MHCII expression, and we defined pro-healing M2 macrophages as $CD45^+CD11b^+F4/80^+$ cells expressing high levels of IL4Rα, Arg-1, CD206, and IL-10[15–17]. We observed no increase in M1 macrophage infiltration 10 days post-RT; however, a significant increase in M2 macrophage infiltration was observed with tumor cell recruitment (**Figure 1B, Figures S1C, D**). In clinical studies of triple negative breast cancer patients, higher numbers of tumor associated macrophages typically with an M2 phenotype are correlated with poorer prognosis in triple negative breast cancer[18]. Expression of CD163, an M2 marker, in breast cancer tumors was linked to increased likelihood of early distant recurrence and decreased overall survival[19]. Additionally, it has been shown that M2 macrophages play a role in radiation-induced recurrence. For example, expression of CD163 in primary head and neck cancer tumors is associated with a higher likelihood of recurrence after RT[20].

Because communication between damaged tissue and immune cells is essential to the wound healing response, we evaluated how local and systemic cytokine expression influenced tumor cell recruitment. Local and systemic cytokine secretion 10 days post-RT from MFP homogenates and mouse serum, respectively, was evaluated using a Luminex multiplex immunoassay. Median fluorescent intensity (MFI) values were normalized to those obtained from mice without tumor cell infiltration or RT. MFPs with tumor cell infiltration post-RT exhibited greater

than a 2-fold increase in interleukin 6 (IL-6) and IL-23, and more than a 3-fold increase in transforming growth factor beta (TGF-β) relative to a mouse without tumor cell infiltration (**Figure 1C**). Additionally, increases in IL-6 expression were observed systemically (**Figure 1D**). Increased levels of IL-6 in serum are associated with higher risk of early recurrence and bone metastasis[21]. Although IL-6 has been traditionally known as a pro-inflammatory cytokine[22], it has been shown to promote TNBC epithelial-mesenchymal transition, progression, cancer stemness, and M2 macrophage polarization[23]. The role of M2 secreted IL-6 as a response to neuroinflammation may be similar to the response of M2 macrophages in an irradiation-damaged normal tissue microenvironment[24]. Together, this data indicates that IL-6 plays a role in the recruitment of circulating tumor cells *in vivo*.

Primary fibroblast spheroid model

The stroma in the mammary gland is made up of a heterogeneous collection of fibroblasts. We evaluated the contributions of cells derived from the mammary stromal vascular fraction (SVF) to tumor cell recruitment. Within 16 hours of plating in U-bottom low-adhesion plates, cells formed spheroids of approximately 300 µm in diameter (**Figure 2A**), a size that is below the threshold where hypoxia and necrosis may occur[11,25]. Surface markers of primary SVF cells were evaluated. It was determined that the isolated cells expressed high and consistent levels of PDGFRβ, Podoplanin, and CD90.2/Thy1.2 (**Figure 2B, Figure S2A**). Expression of these markers have been shown in both healthy mammary glands and in mammary glands containing cancer associated fibroblasts[26,27]. There was negligible expression of immune, epithelial, and endothelial markers (**Figure S2B**), implying that this model is composed primarily of fibroblasts. Fibroblasts secrete components that can makeup ECM, and radiation induces fibrosis, which results in excess ECM production[28,29]. Previous studies have incorporated primary fibroblasts into spheroids[30]; however, we are the first to study the effects of irradiation on spheroid behavior. We

confirmed ECM deposition by evaluating collagen IV expression in spheroids (**Figure 2C, Figure S2C**).

The irradiated microenvironment facilitates TNBC cell recruitment through direct spheroid-macrophage interactions

Radiation induces significant infiltration of macrophages in normal mammary tissue[5], and excess macrophages can cause tumor growth, metastasis, and recurrence[5,31]. We added bone marrow derived macrophages (BMDMs) to our spheroid model to study how macrophage infiltration influences tumor cell behavior. Other studies have modeled macrophage infiltration using multiple tissue types[32]. Based on the results of our *in vivo* studies, we added macrophages at a proportion of 15% of the overall cells. M0, M1, and M2 macrophages made up 85%, 5%, and 10% of the overall macrophage population, respectively. To recapitulate *in vivo* observations of macrophage infiltration, macrophages were added immediately after irradiation (**Figure S3A-B**). We confirmed infiltration of M1 and M2 macrophages into spheroids after 24 hours (**Figure 3A**) and that macrophages maintained relevant levels of expression of M1 (CD86) markers and M2 (IL4Rα) markers for up to 4 days within the co-culture (**Figure S3C**). We tracked individual cell infiltration via live cell imaging (**Figure 3B**). When 4T1 murine TNBC cells were co-cultured with macrophages in irradiated spheroids, they showed significantly higher motility toward the center of the spheroid. GFP intensity in the inner core of the spheroid was normalized to the overall GFP intensity of the spheroid after 24 hours of infiltration (**Figure 3C**). In the case of 2:1 M2:M1 macrophages, interior GFP intensity significantly increased, indicating that 4T1 cells were more migratory when cultured in spheroids that recapitulate a microenvironment that has been shown to facilitate tumor cell recruitment *in vivo*[5]. Additionally, GFP intensity was measured as a function of radial distance from the center (**Figure 3D**). After 72 hours of co-culture, GFP intensity closer to the interior of the spheroid was significantly increased in irradiated spheroids with macrophages

relative to both the stromal only irradiated and unirradiated controls. These results show that direct interactions between macrophages and the irradiated stroma facilitates 4T1 recruitment.

IL-6 secretion drives 4T1 cell invasiveness

Next, we isolated conditioned media (CM) from the co-culture of macrophages and irradiated cells. We characterized IL-6 secretion from spheroids as a function of irradiation and macrophage infiltration to determine if *in vivo* cytokine secretion is replicated in our model. We observed that infiltration of macrophages (2:1 M2:M1) resulted in a significantly higher secretion of IL-6 relative to spheroids with no macrophage infiltration (**Figure 4A**). Additionally, when macrophages were co-cultured with unirradiated spheroids, we observed no significant changes in IL-6 secretion. Interestingly, the co-culture of M0 macrophages with irradiated spheroids did not change IL-6 secretion (**Figure S3D**). These observations establish the importance of maximizing biological relevance by incorporating multiple macrophage phenotypes into spheroid models. The impact of IL-6 on 4T1 invasiveness was then investigated using a transwell assay. 4T1 invasiveness was significantly higher in 4T1s migrating towards CM from irradiated spheroids with macrophages with higher concentrations of IL-6 relative to CM collected from spheroids with no macrophages (**Figure 4B**). Additionally, neutralization of IL-6 in CM resulted in significantly reduced invasiveness of 4T1 cells. Taken together, this data suggests that interactions between tissue damaged from RT and M2 and M1 macrophages causes secretion of IL-6 that in turn recruits 4T1 cells (**Figure 4C**). Myeloid-derived IL-6 has been reported in 4T1 progression and metastasis[33,34]. However, this is the first report of IL-6 driving 4T1 invasiveness post-RT in the context of recurrence. This work highlights the importance of using 3D spheroid models to elucidate mechanisms of cancer recurrence. Our findings indicate that for TNBC patients vulnerable to recurrence, monitoring serum IL-6 levels may provide prognostic and therapeutic value to improving their outcomes.

Methods

Cell Lines. Luciferase-labeled and GFP expressing 4T1 mouse mammary carcinoma cells were obtained from Dr. Laura L. Bronsart (Stanford University). All cells were cultured at 37°C and 5% CO_2. 4T1 cells were cultured in RPMI-1640 (Gibco) supplemented with 10% heat-inactivated fetal bovine serum and antibiotics (100 U/mL penicillin and 100 mg/mL streptomycin). Cells were used within three passages before injection into mice.

Orthotopic Tumor Studies. Animal studies were performed in accordance with institutional guidelines and animal protocols approved by the Vanderbilt University Institutional Animal Care and Use Committee. Tumor inoculation was performed by injecting 5 x 10^4 4T1 cells in a volume of 50 µL of sterile PBS into the number four inguinal right MFPs of 8- to 10-week old female Nu/Nu or Balb/C mice (Charles River Laboratories). Tumor length and width were measured using digital calipers (Fisher Scientific) beginning one week after tumor inoculation. Tumor volume was calculated as follows: Volume = $(L_1^2 \times L_2)/2$, where L_1 is the smaller diameter of the tumor, and L_2 is the larger diameter.

Luminex Multiplex Cytokine Assay. To assess cytokine profiles at the local site of infiltration, mammary fat pads were harvested and homogenized in 20 mM Tris HCl (pH 7.5) buffer with 0.5% Tween 20, 150 mM NaCl, and protease inhibitor, centrifuged for 10 min at 4ºC, and supernatant was stored at -80°C[35]. Protein content was measured using bicinchoninic acid protein assay (ThermoFisher). For evaluation of systemic cytokine signaling, blood samples were collected via retro-orbital bleed, allowed to clot at room temperature for 30 minutes, then centrifuged for 10 minutes. Serum was then recovered and stored at -80°C. Samples were processed at the Stanford Human Immune Monitoring Center using a mouse 39-plex Affymetrix kit.

Primary Spheroid Generation. Spheroids were generated from primary cells obtained from the stromal vascular fraction in mouse MFPs using previously published techniques[30]. MFPs were harvested and minced with a blade and digested for 40 minutes in a solution of PBS with 20 ug/mL liberase, and antibiotics (100 U/mL penicillin and 100 mg/mL streptomycin). Tissue was flushed through a 100 µm filter and plated in 10 cm dishes in DMEM/20% BCS. Upon confluence, cells were plated in low adhesion U-bottom plates at a density of 10,000 cells/spheroid. Spheroids were formed within 24 hours of passaging.

Radiation. Ionizing radiation was delivered in two different methods. For *in vivo* RT, ionizing radiation was delivered to a dose of 20 Gy using a 300 kVp cabinet x-ray system filtered with 0.5 mm Cu. Mice were anesthetized by administering isoflurane. The mice were shielded using a Cerrobend jig with apertures 1 cm wide and 1.5 cm long to expose normal MFPs. Transmission through the 2 cm thick shield was less than 1%. For *in vitro* experiments, spheroids were irradiated in the U-bottom low adhesion plates to a 20 Gy dose using a Cesium source.

Flow Cytometry. MFPs were harvested and minced in a solution of 1% FBS in PBS. They were then placed in a 2 mg/mL solution of Collagenase II (Sigma) and incubated for 30 minutes in a water bath at 37°C. The digestion was inactivated by adding 1% FBS in PBS. The digested tissue was then passed through a 100 µm filter to generate a single cell suspension. Cells were stained with the Aqua fixable viability stain (ThermoFisher) and FC receptors were blocked with CD16/32 (Biolegend) simultaneously with other cell surface markers for 20 minutes at 4°C. After staining, cells were rinsed with PBS and fixed with 1% neutral buffered formalin in saline for at least 20 minutes at 4°C. Intracellular stains were performed using an intracellular permeabilization buffer (ThermoFisher). Flow cytometry was performed on an in-house four-laser CellStream machine, and FlowJo software was used for analysis. Compensations were obtained by using compensation beads (ThermoFisher). The following antibody clones were used for analysis:

CD45 (30-F11), CD11b (M1/70), F4/80 (BM8), MHCII (M5/114.15.2), iNOS (CXNFT), CD64 (X54-5/7.1), CD86 (GL1), CD206 (C068C2), IL-4Rα (I015F8), IL-10 (JES5-16E3), and Arg-1 (A1exF5). For staining of primary SVF cells, cells were passaged and stained using the same staining protocol. The following antibody clones were used for analysis: PDGFRα (APA5), PDGFRβ (APB5), Podoplanin (8.1.1), CD26 (H194-112), and CD90.2/Thy1.2 (53-2.1).

Spheroid Embedding, Sectioning, and Immunofluorescence. Spheroids were stained using previously published methods[36,37]. Tissues were carefully transferred to microcentrifuge tubes using wide bore pipet tips. Spheroids were rinsed 3x in PBS. They were then fixed in 10% Neutral Buffered Formalin overnight at 4ºC. They were rinsed 3x in PBS, then incubated in 30% sucrose overnight at 4ºC. They were then incubated 2-4 hours in 1:1 mixture of 30% sucrose-PBS and OCT. They were transferred to a mold with OCT and stored at -80ºC. 15 µm sections were generated via sectioning on a cryostat (Leica). For immunofluorescence, slides were incubated in PBS to remove the OCT. Then, they were permeabilized with 0.1% Triton-X 100 in PBS for 10 minutes. Sections were then rinsed with PBS, and blocked with 1% BSA in PBS with 10% Normal Goat Serum for 1 hour. Sections were then incubated with primary antibody diluted in 1% BSA in PBS overnight in humid chambers at 4°C. After rinsing with PBS, sections were incubated with secondary antibody diluted in 1% BSA in PBS for 2 hours in humid chambers. Then, after additional PBS rinses, sections were incubated with phalloidin (ThermoFisher) for 1 hour. Coverslips were mounted onto slides using NucBlue mounting media (ThermoFisher) and allowed to cure overnight before imaging on a fluorescence microscope (Leica DMi8). Antibodies and stains used for immunofluorescence studies include iNOS (Abcam), CD206 (Abcam), Collagen IV (Abcam), and Phalloidin (ThermoFisher).

Scanning Electron Microscopy. Spheroids were fixed using methods previously published[38]. Briefly, spheroids were carefully transferred from culture plates into a microcentrifuge tube using

a wide bore pipet. Spheroids were washed 3x in 1x PBS. They were then fixed in 2% glutaraldehyde, 4% paraformaldehyde, and 0.1 M sodium cacodylate buffer (pH 7.3), 1 hr at 4C/1% glutaraldehyde in PBS, 15 min at RT. After fixation, spheroids were washed 3x in PBS. They were washed 2x in PBS, then dehydrated in ethanol in a series of 10 minute incubations of 10%, 25%, 50%, EtOH-PBS, 75%, and 90% EtOH-H2O, 2x 100% EtOH at RT. The spheroids were then further dehydrated in 50% EtOH-HMDS, 100% HMDS, and air dried overnight. They were mounted on carbon backed aluminum stubs, sputter coated with gold, and imaged on a Quanta Scanning Electron Microscope.

Primary Macrophage Isolation and Culture. Bone marrow derived macrophages (BMDMs) were cultured using previously published methods[39–41]. Briefly, macrophages were isolated from the femurs of Nu/Nu mice. Femurs were crushed using a mortar and pestle, and the cell suspension was passed through a 40 µm filter. Red blood cells were lysed with an ACK lysis buffer, and macrophage precursors were plated at densities of $1x10^6$ cells/plate in IMDM supplemented with 10% FBS, antibiotics (100 U/mL penicillin and 100 mg/mL streptomycin), and 10 ng/mL macrophage colony stimulating factor (MCSF) on 10 cm low adhesion plates for 7 days for maturation into macrophages. For polarization, media was spiked with LPS and IFN-γ for 24 hours (M1 macrophages) or IL-4 for 48 hours (M2 macrophages).

Invasion Assay. Conditioned media (CM) collected from spheroid and macrophage co-cultures were used as chemoattractants in an *in vitro* transwell migration assay (Corning reduced growth factor Matrigel invasion chamber, 8 µm pore size). Spheroids were irradiated to 20 Gy and then co-cultured with 2:1 M2:M1 macrophages. Supernatant was collected after 24 hours of co-culture. 100,000 4T1 cells were seeded into the upper chambers and incubated with CM for 24 hours. Cells that invaded through Matrigel inserts or migrated through uncoated inserts were stained

with 4',6-diamidino-2-phenylindole (DAPI) and counted. Invasion was calculated by dividing invasion counts by migration counts.

Spheroid 4T1 Migration Assay. 24 hours after irradiation, 100 GFP-labeled 4T1 cells were plated per spheroid. Infiltration was monitored via live cell fluorescence and phase contrast imaging every 24 hours for a total of 72 hours after plating of 4T1 cells. GFP signal was evaluated as a function of radial position via a custom MATLAB (MathWorks) script. Along the radial axis, 1,000 readings of fluorescent intensity were evaluated over every angle of each spheroid. Readings were normalized to the overall length of each radius to generate relative intensity values. For each biological replicate, more than 10 technical replicates were analyzed.

IL-6 Quantification. IL-6 secretion in CM was measured using an ELISA assay (R&D systems) per manufacturer instructions.

Statistical Analysis. To determine statistical significance, differences in radiation dose on flow cytometry data and cytokine concentration were analyzed using two-tailed unpaired t-tests. One-Way ANOVA was evaluated when comparing co-culture conditions for GFP intensity, IL-6 secretion, and 4T1 invasiveness. All statistical analysis was performed in GraphPad Prism 9.

Acknowledgments

The authors thank Dr. Laura L. Bronsart for providing the GFP- and luciferase-labeled 4T1 cells, Dr. Michael Freeman for irradiator use, Dr. Austin Kirschner and the radiation physics staff for constructing the Cerrobend shield, and Dr. Craig L. Duvall for IVIS use. We also thank the Vanderbilt Cell Imaging Shared Resource (CISR) core for SEM imaging and the Translational Pathology Shared Resource (TPSR) for IF sample preparation. This research was financially supported by NIH grants #R00CA201304, F31CA254311 (B. H.), S10RR026373 (CISR), and

P30CA068485 (TPSR) as well as the Breast Cancer Alliance Young Investigator Grant. Schematics were prepared by the authors using BioRender.

References

1. Siegel, R. L., Millder, K. D., Fuchs, H. E. & Jemal, A. Cancer statistics , 2022. *CA. Cancer J. Clin.* **72**, 7–33 (2022).

2. Adkins, F. C. *et al.* Triple-negative breast cancer is not a contraindication for breast conservation. *Ann. Surg. Oncol.* **18**, 3164–3173 (2011).

3. Dragun, A. E., Pan, J., Rai, S. N., Kruse, B. & Jain, D. Locoregional recurrence in patients with triple-negative breast cancer: preliminary results of a single institution study. *Am. J. Clin. Oncol. Cancer Clin. Trials* **34**, 231–237 (2011).

4. Lowery, A., Kell, M., Glynn, R., Kerin, M. & Sweeney, K. Locoregional recurrence after breast cancer surgery : a systematic review by receptor phenotype. *Breast Cancer Res. Treat.* **133**, 831–841 (2012).

5. Rafat, M. *et al.* Macrophages promote circulating tumor cell-mediated local recurrence following radiotherapy in immunosuppressed patients. *Cancer Res.* **78**, 4241–4252 (2018).

6. Sherry, A. D. *et al.* Systemic Inflammation after Radiation Predicts Locoregional Recurrence, Progression, and Mortality in Stage II-III Triple-Negative Breast Cancer. *Int. J. Radiat. Oncol.* (2019) doi:10.1016/j.ijrobp.2019.11.398.

7. Adra, J. *et al.* Distribution of Locoregional Breast Cancer Recurrence in Relation to Postoperative Radiation Fields and Biological Subtypes. *Int. J. Radiat. Oncol.* **105**, 285–295 (2019).

8. Barcellos-Hoff, M. H. & Ravani, S. A. Irradiated mammary gland stroma promotes the expression of tumorigenic potential by unirradiated epithelial cells. *Cancer Res.* **60**, 1254–1260 (2000).

9. Zheng, Z., Jia, S., Shao, C. & Shi, Y. Irradiation induces cancer lung metastasis through activation of the cGAS–STING–CCL5 pathway in mesenchymal stromal cells. *Cell Death Dis.* **11**, (2020).

10. Ahn, G. O. & Brown, J. M. Matrix metalloproteinase-9 Is required for tumor vasculogenesis but not for angiogenesis: role of bone marrow-derived myelomonocytic cells. *Cancer Cell* **13**, 193–205 (2008).

11. Hacker, B. C. & Rafat, M. Organoids as Complex In Vitro Models for Studying Radiation-Induced Cell Recruitment. *Cell. Mol. Bioeng.* **13**, 341–357 (2020).

12. Hacker, B. C., Gomez, J. D., Silvera Batista, C. A. & Rafat, M. Growth and characterization of irradiated organoids from mammary glands. *J. Vis. Exp.* (2019) doi:10.1021/acssynbio.5b00266.Quantitative.

13. Bagley, J. A., Reumann, D., Bian, S., Lévi-Strauss, J. & Knoblich, J. A. Fused cerebral organoids model interactions between brain regions. *Nat. Methods* **14**, 743–751 (2017).

14. Wang, F. *et al.* Reciprocal interactions between β1-integrin and epidermal growth factor receptor in three-dimensional basement membrane breast cultures: A different perspective in epithelial biology. *Proc. Natl. Acad. Sci.* **95**, 14821–14826 (1998).

15. Ma, R. Y. *et al.* Monocyte-derived macrophages promote breast cancer bone metastasis outgrowth. *J. Exp. Med.* **217**, (2020).

16. Sommerfeld, S. D. *et al.* Interleukin-36gamma-producing macrophages drive IL-17 mediated fibrosis. *Sci. Immunol.* **4**, 1–13 (2019).

17. Yurdagul, A. *et al.* Macrophage Metabolism of Apoptotic Cell-Derived Arginine Promotes Continual Efferocytosis and Resolution of Injury. *Cell Metab.* **31**, 518-533.e10 (2020).

18. Stovgaard, E. S., Nielsen, D., Hogdall, E. & Balslev, E. Triple negative breast cancer–prognostic role of immune-related factors: a systematic review. *Acta Oncol. (Madr).* **57**, 74–82 (2018).

19. Shabo, I., Stål, O., Olsson, H., Doré, S. & Svanvik, J. Breast cancer expression of CD163, a macrophage scavenger receptor, is related to early distant recurrence and reduced patient survival. *Int. J. Cancer* (2008) doi:10.1002/ijc.23527.

20. Balermpas, P. *et al.* Head and neck cancer relapse after chemoradiotherapy correlates with CD163+ macrophages in primary tumour and CD11b+ myeloid cells in recurrences. *Br. J. Cancer* **111**, 1509–1518 (2014).

21. Noman, A. S. *et al.* Serum sonic hedgehog (SHH) and interleukin- (IL-6) as dual prognostic biomarkers in progressive metastatic breast cancer. 1–12 (2017) doi:10.1038/s41598-017-01268-4.

22. Kaur, S., Bansal, Y., Kumar, R. & Bansal, G. Bioorganic & Medicinal Chemistry A panoramic review of IL-6 : Structure , pathophysiological roles and inhibitors. *Bioorg. Med. Chem.* **28**, 115327 (2020).

23. Weng, Y. *et al.* MCT-1/miR-34a/IL-6/IL-6R signaling axis promotes EMT progression, cancer stemness and M2 macrophage polarization in triple-negative breast cancer. 1–15 (2019).

24. Casella, G. *et al.* IL4 induces IL6-producing M2 macrophages associated to inhibition of neuroinflammation in vitro and in vivo. *J. Neuroinflammation* 1–10 (2016) doi:10.1186/s12974-016-0596-5.

25. Däster, S. *et al.* Induction of hypoxia and necrosis in multicellular tumor spheroids is associated with resistance to chemotherapy treatment. **8**, 1725–1736 (2017).

26. Venning, F. A. *et al.* Deciphering the temporal heterogeneity of cancer-associated fibroblast subpopulations in breast cancer. *J. Exp. Clin. Cancer Res.* **40**, 1–21 (2021).

27. Sebastian, A. *et al.* Single-Cell Transcriptomic Analysis of Heterogeneity in Breast Cancer. *Cancers (Basel).* **12**, E1307 (2020).

28. Deleon-Pennell, K. Y., Barker, T. H. & Lindsey, M. L. Fibroblasts : The arbiters of extracellular matrix remodeling. *Matrix Biol.* **91**–**92**, 1–7 (2020).

29. Macarak, E. J., Rosenbloom, J., Joan, T., Biology, C. & Jefferson, T. Therapeutic Approaches to Radiation-Induced Fibrosis. *J Cancer Treat. Diagn* **2**, 7–9 (2018).

30. Taylor, J. *et al.* Generation of immune cell containing adipose organoids for in vitro analysis of immune metabolism. *Sci. Rep.* **10**, 1–14 (2020).

31. Chen, Y. *et al.* Tumor-associated macrophages: an accomplice in solid tumor progression. 1–13 (2019).

32. Kuen, J., Darowski, D., Kluge, T. & Majety, M. Pancreatic cancer cell/fibroblast co-culture induces M2 like macrophages that influence therapeutic response in a 3D model. *PLoS One* **12**, 1–19 (2017).

33. Oh, K. *et al.* A mutual activation loop between breast cancer cells and myeloid-derived suppressor cells facilitates spontaneous metastasis through IL-6 trans-signaling in a murine model. (2013).

34. Radharani, N. N. V, Yadav, A. S., Nimma, R., Kumar, T. V. S. & Bulbule, A. Tumor - associated macrophage derived IL - 6 enriches cancer stem cell population and promotes breast tumor progression via Stat - 3 pathway. *Cancer Cell Int.* 1–19 (2022)

doi:10.1186/s12935-022-02527-9.

35. Benesch, M. G. *et al.* Tumor-induced inflammation in mammary adipose tissue stimulates a vicious cycle of autotaxin expression and breast cancer progression. *FASEB J* **29**, 3990–4000 (2015).

36. Horder, H. *et al.* Bioprinting and Differentiation of Adipose-Derived Stromal Cell Spheroids for a 3D Breast Cancer-Adipose Tissue Model. (2021).

37. Alessandri, K., Ranjan, B., Valérïévitch, V. & Sinha, B. Cellular capsules as a tool for multicellular spheroid production and for investigating the mechanics of tumor progression in vitro. **110**, 14843–14848 (2013).

38. Sachs, N. *et al.* Long-term expanding human airway organoids for disease modeling. *EMBO J.* **38**, e100300 (2019).

39. Francke, A. *et al.* Generation of Mature Murine Monocytes from Heterogeneous Bone Marrow and Description of Their Properties. (2011) doi:10.1369/0022155411416007.

40. Zhang, X., Goncalves, R. & Mosser, D. M. The Isolation and Characterization of Murine Macrophages. *Curr Protoc Immunol* 1–18 (2008) doi:10.1002/0471142735.im1401s83.The.

41. Ying, W., Cheruku, P. S., Bazer, F. W., Safe, S. H. & Zhou, B. Investigation of Macrophage Polarization Using Bone Marrow Derived Macrophages. 1–8 (2013) doi:10.3791/50323.

Figures

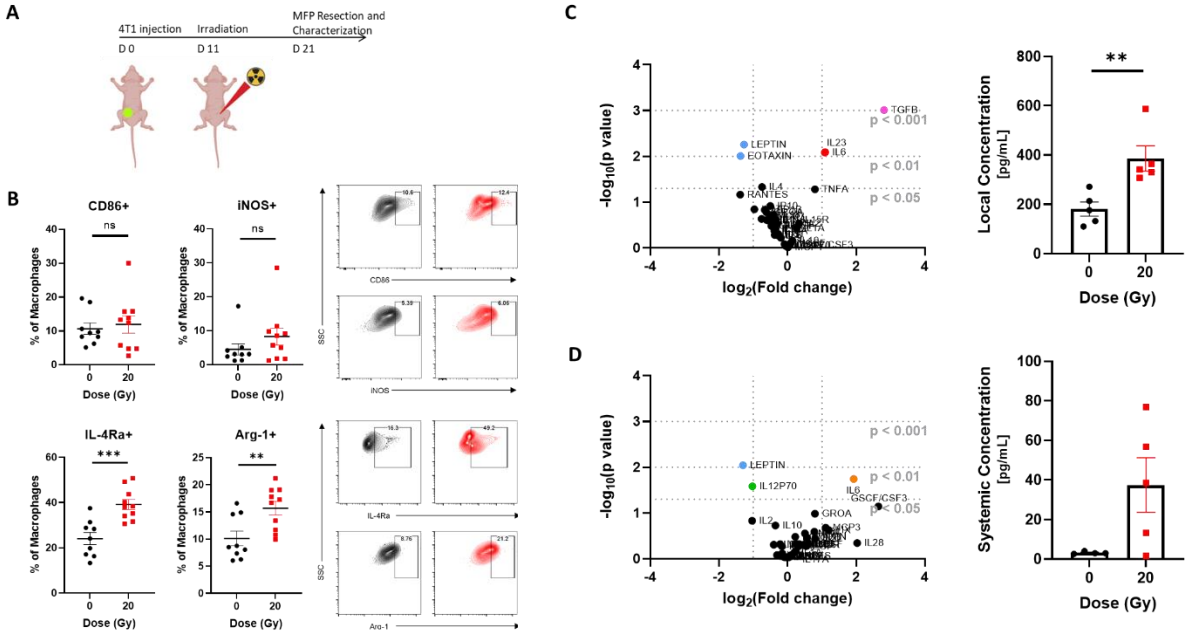

Figure 1. M2 macrophage Infiltration and secreted inflammatory cytokines are increased following *in vivo* RT of mammary tissue. A. Experimental schematic of *in vivo* studies. **B.** Flow cytometry characterization of M1 and M2 macrophage infiltrate 10 days post-RT. **C.** Volcano plot of relative change in cytokines in irradiated MFPs. Differences were calculated by normalizing cytokine MFI values 10 days post-RT to values from baseline healthy immunocompetent mice. **D.** Volcano plot of relative change in cytokines in serum samples. Error bars show standard error of the mean with **p<0.01, ***p<0.001 as determined by a two-tailed unpaired t-test.

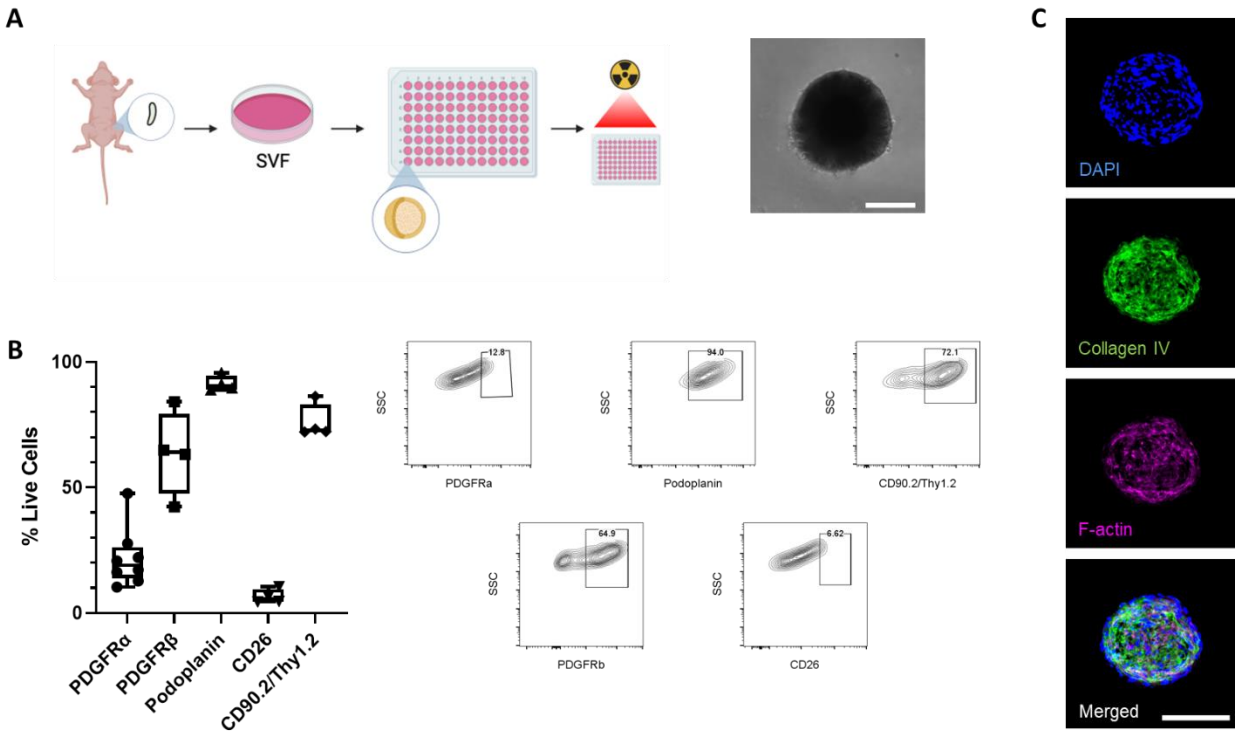

Figure 2. Primary mammary spheroids are composed of fibroblasts and produce ECM. A. Experimental schematic of stromal vascular fraction (SVF) isolation from mouse MFPs, expansion, and irradiating. Representative image of spheroid. Scale bar is 100 µm. **B.** SVF cells are of a fibroblast lineage based on flow cytometry characterization. Data is presented as a box and whiskers plot, with the minimum, maximum, first quartile, median, and third quartile shown. **C.** Upon self-assembly, spheroids produce ECM. Spheroids were stained for collagen IV (green) and F-actin (magenta). Scale bar is 200 µm.

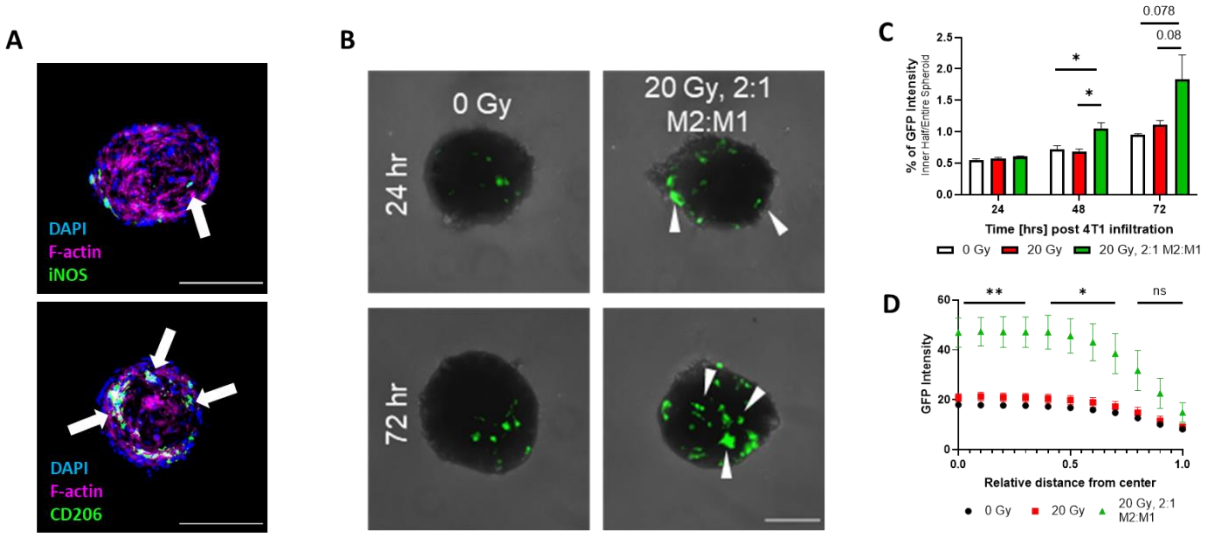

Figure 3. Cell infiltration into spheroids is enhanced by co-culture of irradiated stroma and infiltrating macrophages. A. M1 (iNOS) and M2 (CD206) macrophages infiltrate into spheroids within 24 hours. F-actin was used to stain the cytoskeleton. **B.** GFP-labeled 4T1 infiltration was tracked at 24 and 72 hours following co-culture with spheroids. Infiltration was enhanced in the presence of 2:1 M2:M1 macrophages co-cultured with irradiated spheroids. **C.** GFP signal from 4T1s is enhanced in the interior of the spheroid over time (n=3-4 biological replicates). Interior spheroid GFP intensity was normalized to the total GFP intensity within the entire spheroid at 24 hours of co-culture. **D.** GFP intensity as a function of radial distance at 72 hours. Error bars show standard error of the mean with *p <0.05 and ** p <0.01 as determined by a two-tailed unpaired t-test. Scale bars are 200 μm.

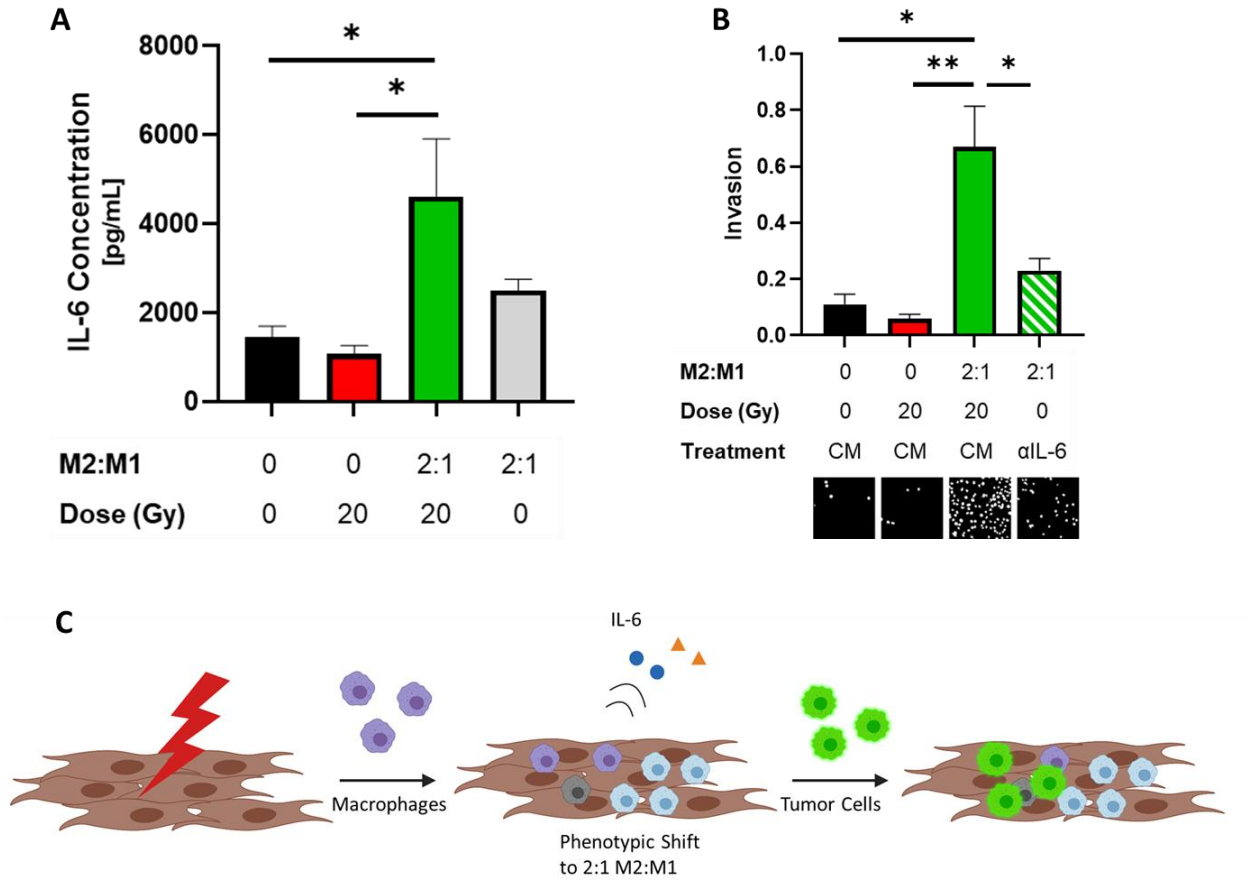

Figure 4. IL-6 secretion drives tumor cell invasion *in vitro*. A. Spheroid conditioned media (CM) incubated for 24 hours after RT promotes IL-6 secretion when cultured with a 2:1 ratio of M2:M1 macrophages (green). IL-6 secretion is lower in the absence of spheroid RT (black), with spheroid RT and no macrophage infiltration (red), or with macrophage co-culture without RT (gray). **B.** IL-6 secreted from RT spheroids co-cultured with macrophages promotes 4T1 cell invasion. IL-6 neutralization (αIL-6, striped green) of the CM diminished invasion. Error bars show standard error of the mean with *$p<0.05$ and **$p<0.01$ as determined by ANOVA analysis. **C.** Proposed mechanism of 4T1 tumor cell infiltration following normal tissue RT.